Biosensors and Bioelectronics 144 (2019) 111676

Contents lists available at ScienceDirect

Biosensors and Bioelectronics

journal homepage: www.elsevier.com/locate/bios

Highly-branched Cu_2O as well-ordered co-reaction accelerator for amplifying electrochemiluminescence response of gold nanoclusters and procalcitonin analysis based on protein bioactivity maintenance

Yue Jia, Lei Yang, Jingwei Xue, Xiang Ren, Nuo Zhang, Dawei Fan, Qin Wei, Hongmin Ma*

Key Laboratory of Interfacial Reaction & Sensing Analysis in Universities of Shandong, School of Chemistry and Chemical Engineering, University of Jinan, Jinan, 250022, China

ARTICLE INFO

Keywords:
Electrochemiluminescence biosensor
Bioactivity-maintenance
Au NCs
Cu_2O
Co-reaction acceleration

ABSTRACT

The point of fabricating ultrasensitive electrochemiluminescence (ECL)-based biosensors should be focused on how to maintain high immune recognition of antigens by antibodies in whole process. That is not effortless due to the structure of the protein can be destroyed root in toxic nanocarriers, excessive cyclic potential and superoxide radicals in coreactant, all of which can lead to reduce the bioactivity of antigen and antibody. In this work, the effect of negative voltage and divers coreactant on protein bioactivity were verified. Based on that, a motivated ECL biosensor with good biocompatibility was fabricated for procalcitonin (PCT) detection using Au nanoclusters (Au NCs) as low-potential cathodic luminophor and $K_2S_2O_8$ as non-toxic coreactant, respectively. Besides, highly-branched Cu_2O was utilized to catalyze $K_2S_2O_8$ and produce more radical anion $SO_4^{\bullet -}$, which can oxidize Au $NCs^{\bullet -}$ to generate more high-energy-state Au NCs*, thus doubling the ECL intensity to meet the requirements of trace analysis. In addition, protein A (PA) as specific antibody capturer was employed to bind the Fc region of anti-PCT in an orientated way, further maintaining the physiological activity of antibody. As expected, all strategies undoubtedly practically improved the immune recognition of the biosensor and reduced the detection limit to 2.90 fg/mL.

1. Introduction

As key component of electrochemical immunoassay tools, electrochemiluminescence (ECL) possesses distinctive advantages of low background noise, good controllability, abundant signal labels and so on, has been widely focused (Chen et al., 2019; Sun et al., 2019; Yan et al., 2019a). In particular, the implementation of trace analyses of some low-abundance biomarkers have resulted in lower incidence of related diseases (Li et al., 2019; Yan et al., 2019b). But rationally, many researchers seem to be in a dilemma in the process of expanding ECL technology to immunoassay, and the reason is more attention is paid to excavate new ECL emitters or derivatives of traditional ECL materials, while the key point of protein activity in immunoassay is ignored (Jia et al., 2019b; Makaraviciute and Ramanaviciene, 2013). Beyond doubt, the immune recognition of biosensors depends on the bioactivity of immobilized molecules, while the bioactivity of antigens or antibodies may be affected by experimental conditions, such as excitation potential, scanning time and toxicity of nanocarriers or coreactant (Bruce and Richter, 2002; Davies, 1987). For example, an affinity reaction could occur between Cd-based materials and variety functional groups (hydroxyl, amino and hydrosulfuryl) provided by antibody molecules to form cadmium protein, which almost has no bioactivity (Zhao et al., 2017). Reactive oxygen species (ROSs) such as superoxide radicals ($O_2^{\bullet -}$) produced by H_2O_2 or dissolved oxygen as coreactant can cause irreversible oxidative damage to oligonucleotides (Cabiscol et al., 2000; Davies, 1987). In view of increasing number of such reports, focusing energy on the research of new sensing strategies to replace unboundedly exploring more ECL emitters can improve ECL immunoassay to a new level.

Gold nanoclusters (Au NCs), a traditional fluorescent indicator, have become ideal ECL emitter in immunoassay due to its size-tunable luminescence and high quantum yield (Yan et al., 2018; Yang et al., 2019b). In particular, bovine serum albumin (BSA)-templated Au NCs with good biocompatibility not only function as signal label for the indication of target concentration, but also act as connector for the modification and fixation of immune molecules via abundant functional groups provided from BSA (Zhang et al., 2019b). However, the relatively low ECL efficiency is always the main obstacle for its better

* Corresponding author.
E-mail address: mahongmin2002@126.com (H. Ma).

https://doi.org/10.1016/j.bios.2019.111676
Received 26 July 2019; Received in revised form 22 August 2019; Accepted 3 September 2019
Available online 10 September 2019
0956-5663/

application and the reason is that the mass transport and electron transfer could be limited root in the poor conductivity of protein (Zhou et al., 2018). While trace analysis emphasizes that the luminous intensity of ECL-based biosensor should be within a reasonable range, thus some promotion strategies should be introduced to double the signal intensity.

To date, the ECL emitter of semiconductor quantum dots utilizing $S_2O_8^{2-}$ as coreactant has yield satisfactory achievements (Sha et al., 2019). It could be electrochemically reduced to produce the oxidant intermediates of $SO_4^{\bullet-}$, which could then react with the negatively charged Au $NCs^{\bullet-}$, by injecting a hole into the highest occupied molecular orbital to induce an excited state of Au NCs*, releasing optical signal (Ma et al., 2015). Thus, stronger ECL response depends on the amount of $SO_4^{\bullet-}$ mediators. Indeed, raising the concentration of $S_2O_8^{2-}$ seems to be a feasible method to improve production of $SO_4^{\bullet-}$ (Wang et al., 2019). But this purpose is hard to be achieved due to the commonplace solubility of $S_2O_8^{2-}$ and the nonlinear relationship between the concentration of $S_2O_8^{2-}$ and $SO_4^{\bullet-}$ (Ma et al., 2015). The expansion of co-reaction acceleration strategy to ECL system could effectively conquer this issue (Yu et al., 2016). There are many reports of this, especially iron and copper-based compounds with excellent redox property, which can interact with coreactant to improve the formation of intermediate free radicals, accelerating the ECL excitation (Song et al., 2019; Zeng et al., 2018).

Inspired by the above description, the proposition of the effect of several common coreactant and negative potential on protein bioactivity was initially verified. In view of this fact, the Au NCs with good biocompatibility was selected as low-potential cathode signal label and non-toxic $S_2O_8^{2-}$ as coreactant for procalcitonin (PCT) detection. In order to offset the weak optical signal of the system, highly-branched Cu_2O was employed as a co-reaction accelerator to catalyze $S_2O_8^{2-}$, producing more $SO_4^{\bullet-}$ intermediates and accelerating ECL excitation. Compared the widespread electrode modification with dripping coat approach, electroplated Cu_2O can evenly and firmly adhere to the surface of indium tin oxid (ITO). With a sufficient dense of oriented Cu_2O, all the exposed active sites became effective for ECL emission enhancement due to the improved electron-transport along the ordered array structure. In addition, protein A (PA), utilizing as a powerful site-oriented antibody capturer with superiority of low cost to construct a well-ordered specific sensing interface, can improve the availability of incubate antigen effectively. As expected, all protective strategies towards antibody or antigen undoubtedly improved the immune recognition of the biosensor, and the detection limit of the target PCT was as low as 2.90 fg/mL, which will be of great significance to the application and development of biosensors in future.

2. Experimental section

Materials, reagents and apparatus are provided in the Supplementary Material.

2.1. Preparation of well-ordered Cu_2O sensing base substance

Before plating, the pretreatment of ITO electrodes should be done. All ITO electrodes were cut into the size of 1×2 cm and sonicated in acetone and ethanol, respectively. After thoroughly cleaned with ultrapure water, the dustless electrodes were dried in nitrogen (N_2) atmosphere. Then, the well-ordered Cu_2O layer was prepared using a standard three-electrode system in electrolyte composed of 0.1 M NaAc and 0.02 M $Cu(Ac)_2$ aqueous solutions with stirring about 300 rpm, which controlled by a magnetic stirrer. The chronoamperometry was used with a potential of -0.2 V for 40 s at room temperature (Sun and Wang, 2019). After deposition, such Cu_2O films were rinsed with ultrapure water and dried with N_2 for further use.

2.2. Preparation of BSA-templated Au NCs

The synthesis of Au NCs followed the procedure described in previous reports with minor changes. 5 mL of 0.2 wt% $HAuCl_4$ aqueous solution mixed with BSA solution (5 mL, 50 mg/mL) and kept uniform stirring for 10 min. After the pH of above solution adjusted to 12 with NaOH, the mixture was kept 37 °C overnight (Xie et al., 2009). Finally, the obtained light brown solution was filtered with dialysis membrane (MWCO: 3500 Da) in ultrapure water for 60 h to adjust the Au NCs solution to neutral and kept in 4 °C for further use.

2.3. Preparation of Au NCs/PA/Ab_2 bioconjugates

In view of the large amount of carboxyl groups provided by BSA on Au NCs surface. Amine reaction could occur between carboxyl and amino groups, where come from PA. The specific operation are as follows: 20 μL of 50 μg/mL PA was initially activated using 4 μL of EDC/NHS (5 mg/mL of EDC and 1 mg/mL of NHS) and mixed with the 1 mL of prepared Au NCs solution. After oscillation at 4 °C overnight, the formative Au NCs/PA were separated from the residuum. Then, 100 μL of detection antibody (Ab_2) (5 μg/mL) was incubated with above bioconjugates for 1 h to obtain the purposed product.

2.4. Analysis effect of negative potential and coreactant on PCT bioactivity

To verify the proposition of negative potential or coreactant can damage the protein structure, related experiments were designed. Circular dichroism (CD) spectrum was employed to characterize the conformation change of PCT, and all data of the whole experiment were expressed by the mean residue ellipticity (MRE). Prior to start, it is necessary to emphasize that all PCT samples was bubbled for 30 min with high purity N_2 to ensure emptying all dissolved oxygen, which could disturb testing results via $O_2^{\bullet-}$ produced by redox reactions. Specifically, in the first group, four identical PCT samples (10 mL, 0.5 mg/mL) were stimulated for 30 s under different cycle negative voltages (0, −1–0, −1.2–0, and −1.5–0 V) and the second group of PCT samples were mixed with common coreactant (nothing, 50 mM trimethylamine (TEA), 120 mM $K_2S_2O_8$, and 10 mM H_2O_2) and then stimulated at 0 ~ −1.2 V for 30 s.

2.5. Fabrication of purposed biosensors

The fabrication process of purposed biosensor was graphically exhibited in Scheme 1. Initially, the prepared ITO was functionalized with mercaptoacetic acid (TGA) to introduce carboxyl groups. After activation with 4 μL of EDC/NHS, 5 μL of PA solution (50 μg/mL) was dripped onto the well-ordered Cu_2O surface to couple antibody capturer via amidation. Following that, the dried ITO was immersed in primary antibody (Ab_1) (5 μg/mL). Later, 3 μL of BSA (0.1 wt%) was coated on the formed film to block the remaining nonspecific binding sites. Then, PCT with different concentrations were modified the electrode surface. Finally, the Au NCs/PA/Ab_2 was fixed as signal probe to finish the biosensor fabrication.

2.6. ECL detection of purposed biosensors

The ECL detection was performed in 10 mL electrolyte containing 0.1 M of PBS (pH 8.0) and 120 mM of $K_2S_2O_8$. The ECL signals were excited by a cyclic voltammetry system with the potential range from −1.2–0 V and recorded by the MPI-1 ECL analyzer with the voltage of photomultiplier tube was set at 800 V.

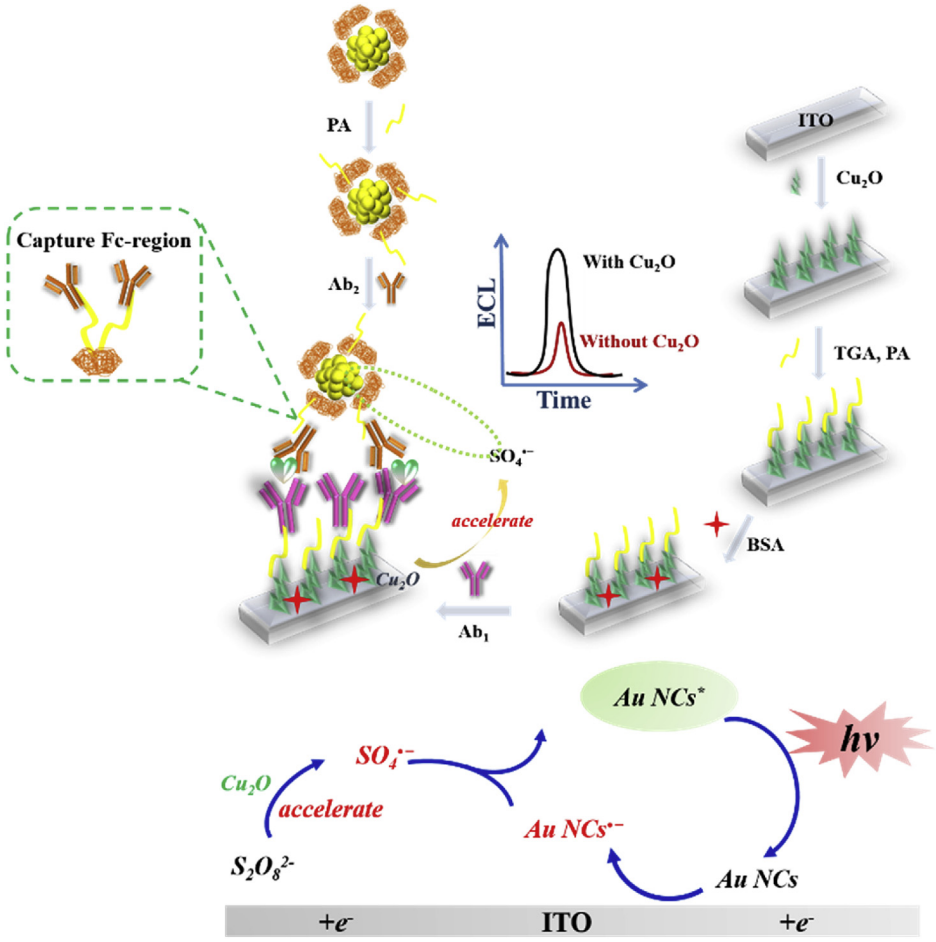

Scheme 1. Fabrication process for the purposed biosensor.

3. Results and discussion

3.1. Characterization of Cu_2O films

The morphologies of Cu_2O films were characterized by scanning electron microscopy (SEM). As shown in Fig. 1A, the well-ordered Cu_2O was uniformly laid on the ITO electrode surface with an average size of 2 μm. Under high magnification (Fig. 1B), the dendric surface with many irregular bulges and folds exhibited large surface area that could provide more binding sites to combine PA. In order to further demonstrate the successful preparation of Cu_2O, the X-ray diffraction (XRD) was used to analyze its crystallization and the result was shown in Fig. 1C. It can be clearly seen that multiple sharp diffraction peaks appeared at $2\theta = 29.98°$, 37.00°, 42.61°, 62.44°, which corresponded to the (110), (111), (200) and (220) planes of Cu_2O, respectively (Sun and Wang, 2019). As for the impurity peaks, they belong to the characteristic peaks of ITO. In view of above results, the Cu_2O was successfully electroplated on the ITO surface.

3.2. Characterization of BSA-templated Au NCs

Transmission electron microscope (TEM) was employed to observe the morphology of Au NCs. Spherical Au NCs enshrouded by BSA exhibited uniform diameters around 2–2.5 nm (Fig. 1D). Moreover, it can be easily measured that the lattice spacing about 0.23 nm, which matched the results from the (111) crystal plane of the Au NCs (Guo et al., 2016). Then, the UV–vis and fluorescence spectra (Fig. 1E) were used to further prove the character of Au NCs. A distinct UV–vis absorption peak was found at 275 nm (blue curve), which could be interpreted as belonging to BSA. It is also proved that have no localized surface plasmon resonance in the absorption range of Au NCs due to nothing peaks appeared at 500–550 nm (Grabar et al., 1997). And then, the fluorescence spectrum showed an emission peak with the wavelength of 700 nm (pink curve), which was consistent with the reported literature (Zhang et al., 2019a). All description can adequately prove the successful Au NCs synthesis.

3.3. Characterization of carboxylic Cu_2O

In order to support that Cu_2O was successfully introduced carboxyl groups by TGA, the Fourier transform infrared spectroscopy (FTIR) was employed to analyze functional groups on Cu_2O surface with different states (Klepper et al., 2011; Nhlapo et al., 2012). As shown in Fig. 1F, the pure Cu_2O has no obvious FTIR absorption (green curve). After functionalization with TGA, the obtained carboxylic Cu_2O had many additional characteristic peaks (blue curve) compared with the original sample. The wide absorption peaks in the range of 2600–3550 cm^{-1} belong to the stretching vibration of O–H. And the absorption peaks at 1243 cm^{-1} and 1419 cm^{-1} represent the deformation vibration of O–H. Distinctly, the sharp double-bond stretching vibration peak of C=O was observed at 1718 cm^{-1}. The results included all characteristic peaks corresponding to carboxyl groups, which confirmed that is feasible to introduce carboxyl groups via this method.

3.4. Motivation analysis of using Au NCs/$S_2O_8^{2-}$ ECL system

It has been reported that oligonucleotides can be oxidized irreversibly under excessive potential or superoxide radical. If true, some ECL

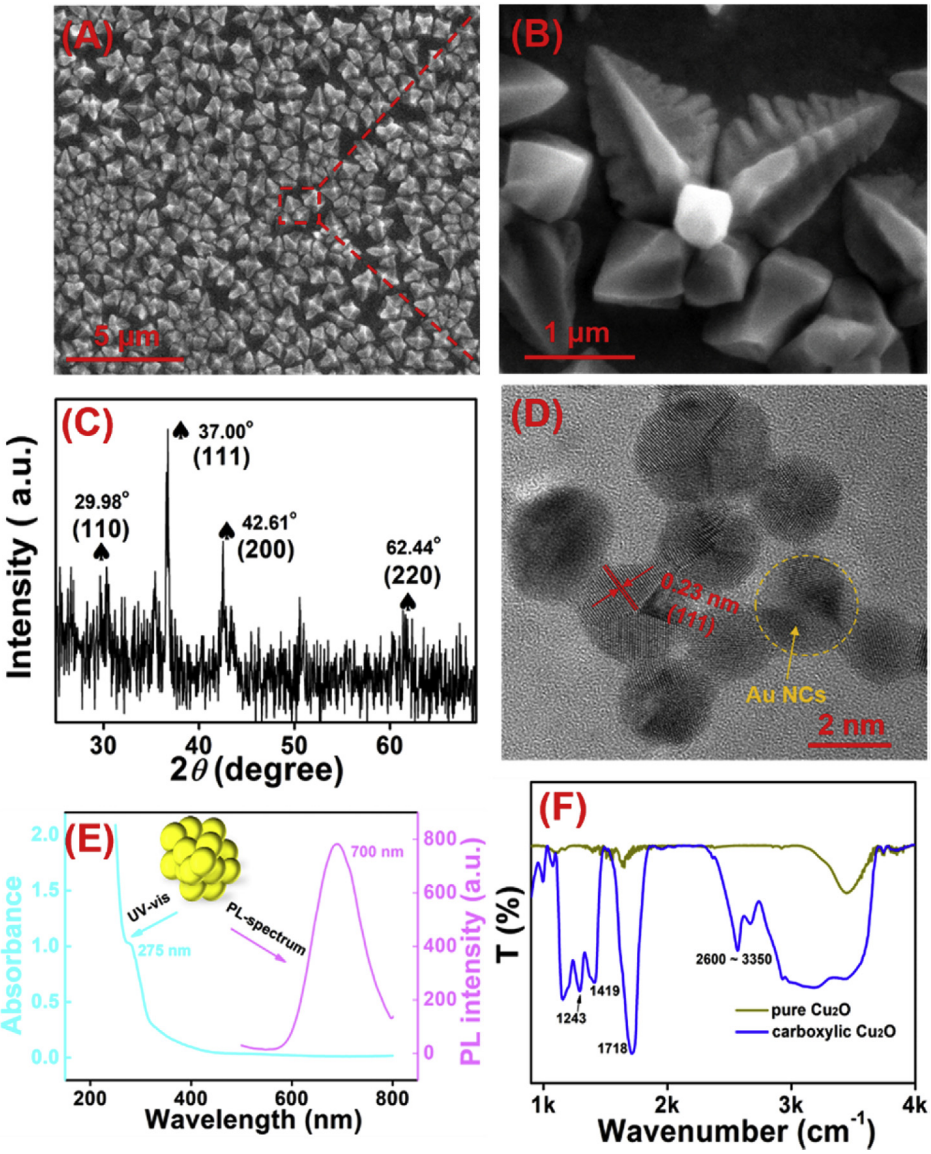

Fig. 1. (A, B) SEM images and (C) XRD pattern of Cu_2O films. (D) TEM image, (E) UV–vis absorbance (blue curve), PL spectrum (pink curve) of Au NCs. (F) FTIR spectra of pure Cu_2O (green curve) and carboxylic Cu_2O (blue curve). (For interpretation of the references to colour in this figure legend, the reader is referred to the Web version of this article.)

luminophors with high-excitation-potential limited to immunoassay application. With concerns, the effect of negative voltage on the bioactivity of PCT was explored, and the results were shown in Fig. 2A. Curve (a) showed the CD spectrum of PBS (pH 8.0), the straight line proved that it is reasonable as solvent. Then, curve (b) corresponds to the CD spectrum of the untreated PCT sample, which showed secondary structure with analogous β-sheet conformation due to the absorption peak at 216 nm (Greenfield, 2006). Compared with other results, this sample showed the largest MRE, which is reasonable and can be used as a reference. Later, the CD absorption of PCT samples stimulated under different potentials (−1–0, −1.2–0, −1.5–0) was detected, which corresponded to the curve (c), (d), (e), respectively. It can be clearly seen that when the potential was reduced to −1.5 V, the MRE of this sample decreased by nearly one third compared to the others with minor changes. These results verified the proposition of the over-potential stimulus could affect protein bioactivity to be true.

As core component of ECL system, coreactant could affect the immune molecule bioactivity via oxidized ions. In this part, the interaction between common coreactant and PCT was explored. As shown in Fig. 2B, no CD absorption (curve a) occurred by detecting the mixture containing TEA, $K_2S_2O_8$ and H_2O_2, which suggested that these substances did not interfere with the following analysis. Curves (c), (d) and (e) represented CD spectra of $K_2S_2O_8$, TEA, H_2O_2 respectively mixed with PCT after CV scanning with potential range from −1.2–0 V. Compared with the CD spectrum of the original PCT (curve b), their MRE showed a gradually decreasing trend. As relevant literature description, when the potential reaches −1.2 V or lower, oxygen evolution reaction can be triggered from H_2O_2, producing $O_2^{\bullet -}$ or other ROS, which can damage protein molecules. As for the PCT conformation changes caused by TEA, it may be based on its unavoidable amine toxicity. In contrast, $K_2S_2O_8$ has little effect on PCT bioactivity. Based on the motivation of protecting immune molecules bioactivity, Au NCs with low-excitation potential was selected as ECL emitter and $K_2S_2O_8$ as relatively non-toxic coreactant.

3.5. ECL enhancement emission of Cu_2O in Au NCs/$S_2O_8^{2-}$ system

In order to control ECL intensity within a reasonable range to meet requirement of trace analysis, a co-reaction acceleration strategy was mentioned using Cu_2O as accelerator. With the purpose of investigating

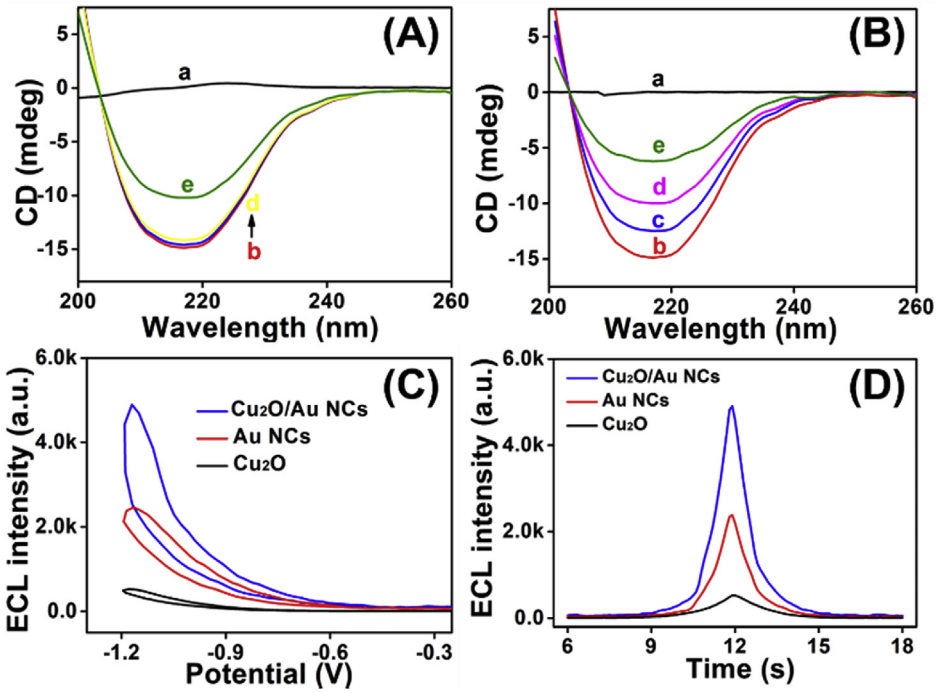

Fig. 2. CD spectra of PCT samples stimulated by negative potential with different range (A) and common coreactant (B). ECL-potential (C) and ECL-time (D) curves of pure Cu_2O (black curve), Au NCs (red curve) and Cu_2O/Au NCs composites (blue curve). (For interpretation of the references to colour in this figure legend, the reader is referred to the Web version of this article.)

positive effects of Cu_2O on ECL enhancements of Au NCs, contrast experiments were implemented through testing the ECL responses of different modified electrodes. As depicted in Fig. 2C and D, the ECL signal generated by Cu_2O/Au NCs (blue curve) was two times higher than that of pure Au NCs (red curve) while almost no signals were excited from pure Cu_2O (black curve). The possible ECL enhancement mechanism was inferred as follows (Guo et al., 2016). With started and deepened cathodic scanning, $S_2O_8^{2-}$ and Au NCs were electrochemically reductive to generate anion radical of $SO_4^{\bullet -}$ and Au NCs$^{\bullet -}$, respectively (eqs (3) and (4)). As reductant, Au NCs$^{\bullet -}$ reacted with oxydic $SO_4^{\bullet -}$ to form the high-energy-state Au NCs* (eq (5)). In the final react process, Au NCs* decayed back to the ground state to finish the ECL emission process (eq (6)). Thus, the amount of $SO_4^{\bullet -}$ directly determines the ECL intensity in the whole process, while Cu_2O could catalyze $S_2O_8^{2-}$ and generate more $SO_4^{\bullet -}$ to accelerate ECL emission (eqs (1) and (2)) (Song et al., 2019).

$$Cu^{+} + S_2O_8^{2-} \rightarrow Cu^{2+} + SO_4^{\bullet -} \text{ (more)} + SO_4^{2-} \quad (1)$$

$$Cu^{2+} + e \rightarrow Cu^{+} \quad (2)$$

$$S_2O_8^{2-} + e \rightarrow SO_4^{\bullet -} + SO_4^{2-} \quad (3)$$

$$\text{Au NCs} + e \rightarrow \text{Au NCs}^{\bullet -} \quad (4)$$

$$SO_4^{\bullet -} + \text{Au NCs}^{\bullet -} \rightarrow \text{Au NCs*} + SO_4^{2-} \quad (5)$$

$$\text{Au NCs*} \rightarrow \text{Au NCs} + h\nu \quad (6)$$

3.6. Optimization of pH in proposed ECL system

pH can not only interfere the signal intensity of ECL system, but also could affect the efficiency of capturing antibody by PA. With the aim of realizing ultrasensitive detection of PCT, the optimal pH of this system was explored. As shown in Fig. 3, the yellow line chart indicated that ECL intensity fluctuated with pH. The strongest signal appeared at pH of 7.5, followed modest decreased in slight. In contrast, the blue histogram showed that the incubation amount of antibody changes with pH. It has been clearly that a significant increase in incubation capacity when the pH jumps from 7.5 to 8.0, which is contrary to the ECL results. Considering that antibody incubation amount depends on the

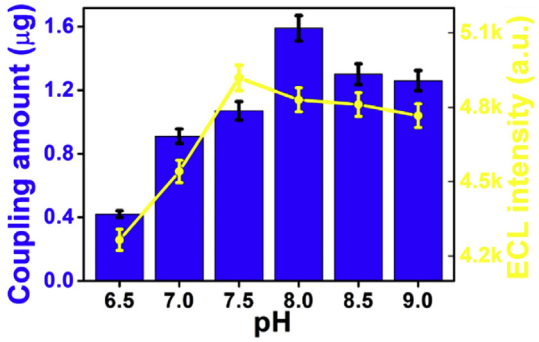

Fig. 3. Effects of pH on ECL intensity and capture efficiency of antibody by PA.

sensitivity of biosensor, and the decrease of ECL signal at pH = 8.0 is minor. Thus, 8.0 was chosen as optimal pH for PCT detection.

3.7. Electrochemistry characterization of biosensor fabrication

Electrochemical impedance spectroscopy (EIS) is one of the most commonly used electrochemical methods to support the stepwise fabrication of the biosensor. Fig. 4A showed the original curves of EIS with different modified ITO electrodes, which were carried out in an electrolyte containing 2.5 mM $[Fe(CN)_6]^{3-/4-}$ and 0.1 M KCl. Curves (a) and (b) represented the EIS of pure Cu_2O and PA-shrouded Cu_2O, respectively. It can be clearly seen that the impedance increased significantly after coating a layer of PA on the Cu_2O surface, what can be explained that PA is a nonconductor and it could block the electrons transfer. With the sequential modification of BSA, Ab_1, PCT and Au NCs-PA-Ab_2, the semicircle domains showed a rising tendency (curves (c) to (f)), indicating higher electron transfer resistance. The experimental results proved the successful fabrication of the biosensor.

CV scanning is an important method to characterize the assembly process of the biosensor, which could clarify the interface properties of the electrodes and further improve the reliability of EIS results. As shown in Fig. 4B, the biosensor with different modification states were tested using CV model in an electrolyte containing 2.5 mM $[Fe(CN)_6]^{3-}$ and 0.1 M KCl. It can be seen that the pure Cu_2O has the largest peak

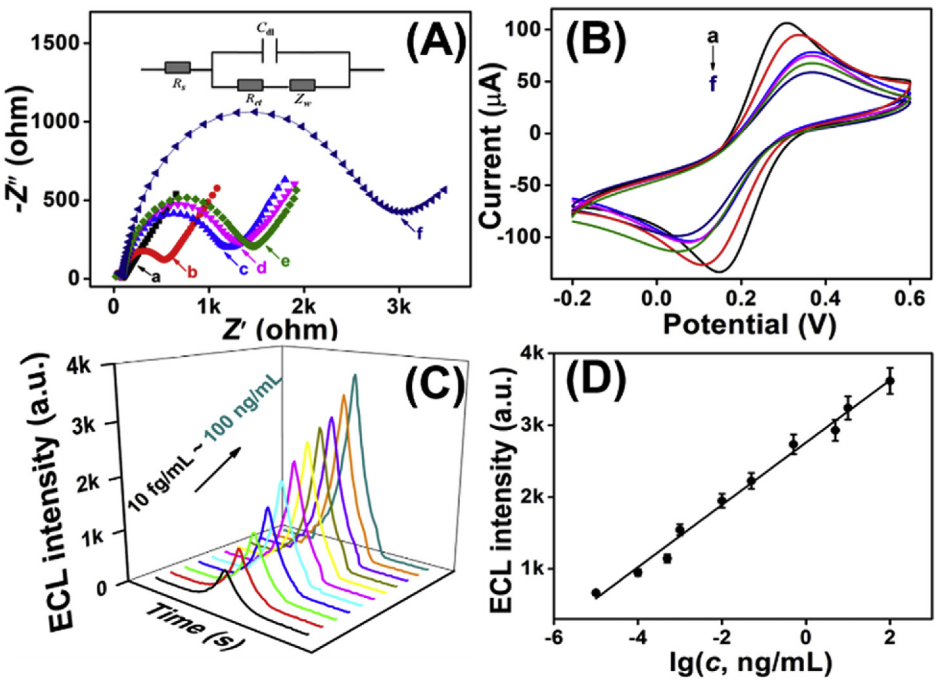

Fig. 4. (A) EIS and (B) CV profiles of stepwise modified electrodes: (a) ITO/Cu_2O, (b) ITO/Cu_2O/PA, (c) ITO/Cu_2O/PA/BSA, (d) ITO/Cu_2O/PA/BSA/Ab_1, (e) ITO/Cu_2O/PA/BSA/Ab_1/PCT, (f) ITO/Cu_2O/PA/BSA/Ab_1/PCT/Au NCs-PA-Ab_2. (C) ECL-time curve and (D) calibration curve of biosensor detected standard PCT with different concentrations: 10 fg/mL, 50 fg/mL, 100 fg/mL, 500 fg/mL, 1 pg/mL, 5 pg/mL, 10 pg/mL, 100 pg/mL, 500 pg/mL, 5 ng/mL, 10 ng/mL, 100 ng/mL.

current. However, as PA, BSA, Ab_1, PCT and Au NCs-PA-Ab_2 with poor electrical conductivity were modified on the electrode surface, the peak current presented a decreasing trend. This indicated that the above substances can be successively bonded to the electrode surface. From what has been discussed above, the proposed biosensor was fabricated successfully.

3.8. ECL response towards PCT

In this work, PCT with different concentrations were detected to analyze the performance of the biosensor under optimal conditions. Fig. 4C exhibited the trend in ECL intensity by detecting a series of PCT with concentrations from 10 fg/mL to 100 ng/mL. The calibration curve (Fig. 4D) was displayed by plotting the logarithm of PCT concentration against the ECL intensity with the equation of $I = 2776 + 434.0 \times \lg c$ (R = 0.995). Upon calculation, the obtained ultralow detection limit was 2.90 fg/mL (S/N = 3), which is far lower than that of other detection methods (Table 1). The above experimental results proved that the biosensor with great sensitivity could achieve the detection of PCT at the femtogram level based on the protein bioactivity maintenance, as expected.

3.9. Performance analysis of biosensor

The clinical application of biosensors requires good specificity and stability. Especially for serum samples with complex composition, the specificity can directly reflect the value of it. In this section, we focused on the specific experiments of interfering antigens, external energy and other factors on the purposed sensor, the results were shown in Fig. 5A. Electrode (1), (2), and (3) represented the ECL signals of fabricated biosensors washed with PBS for 1, 5 and 10 min, respectively. And the results showed no significant difference, which confirmed that the lamination of the biosensors were achieved by covalent bonds and specific immunity, rather than physical adsorption. Then, three common species in serum (CRP, Aβ, ALB) were selected as interferers and modified electrode surfaces as targets in the presence and absence of PCT (electrodes of 4–9). The results showed that they did not interfere with the detection of PCT, indicating that the purposed biosensor had excellent specificity. Operational stability is one of the most important indexes to measure the performance of biosensor. As shown in Fig. 5B, the stability of the ECL biosensor was investigated by detecting 0.1 ng/mL PCT under 12 cycles of successive potential scans. It was calculated that the relative standard deviation (RSD) of ECL intensity was 1.17%, which indicated that the sensing signal was quite reliable. In addition, the repeatability of the ECL biosensor (Fig. S1) was also inspected by detecting six electrodes incubated with PCT (1 ng/mL). With the result of RSD = 1.36%, the proposed ECL biosensors exhibited a favorable reproducibility.

3.10. Trace analysis of PCT in human serum

The detection of pure PCT purchased from biological companies does not fully reflect the potential of biosensor due to the human serum being more complex than it, thus the real serum sample analysis should be included. In this work, the standard addition method was applied (Bi et al., 2017; Jia et al., 2019a). Before that, the serum was obtained from local hospital and its PCT value was provided to be 0.046 ng/mL. The samples were divided into four groups, and each group was spiked with 0.05, 0.1, 0.2, 0.5, 1, 5, 10 ng/mL of PCT standard samples, respectively. As shown in Table 2, the recoveries were acceptable with a

Table 1
Comparison of purposed method with other reported methods for PCT detection.

Reference	Analysis methods	Linear range (ng/mL)	Detection limit (pg/mL)
Li et al. (2014)	ECL biosensor	0.01–20	3.4
Ghrera (2019)	Electrochemical sensor	1–100	210
Shen et al. (2015)	Electrochemical sensor	0.0018–500	0.36
Yang et al. (2019a)	ECL biosensor	0.0001–50	0.041
this work	ECL biosensor	0.00001–100	0.0029

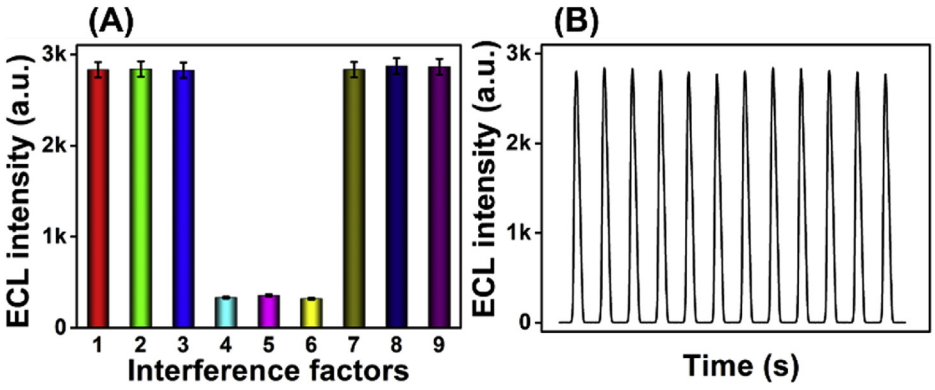

Fig. 5. (A) Specificity test of cathodic ECL signal observed at −1.2 V for 1 ng/mL PCT with different interference factors: the modified electrodes were immersed in PBS for 1 min (1), 5 min (2) and 10 min (3); pure interference of CRP (4), Aβ (5) and ALB (6); the mixture of PCT and the above interferent (7, 8, 9). (B) Stability evaluation of purposed biosensor for 12 cycles.

Table 2
The recoveries of PCT in human serum samples using this biosensor measured in 10 mL PBS (pH = 8.0) containing 120 mM $K_2S_2O_8$.

Simple number	Origin number (ng/mL)	Spiked samples (ng/mL)	Amount found (ng/mL)	RSD (%,n = 3)	Recovery (%)
1	0.046	0.05	0.091	0.66	89.1
2		0.10	0.141	1.09	89.1
3		0.20	0.237	0.47	80.4
4		0.50	0.539	0.87	84.8
5		1.00	1.042	0.51	91.3
6		5.00	5.043	1.41	93.5
7		10.00	10.040	1.29	87.0

satisfying value of 80.4%–93.5%, proving the application potential of this biosensor in detecting PCT in human serum samples.

4. Conclusions

In summary, we suspected and verified that negative potential and coreactant could affect the immune activity of antigen or antibody. Based on this, a novel ECL biosensor was developed using Au NCs with excellent biocompatibility as low-potential emitter and well-ordered Cu_2O as co-reaction accelerator. With a sufficient dense of oriented Cu_2O, all of the exposed active sites became effective for ECL emission enhancement due to the improvement electron-transport along the ordered array structure. Notably, PA endowed the interface a peculiarity to facilitate the incubation process of antibody with a better maintained biological activity, which significantly improved the sensitivity of biosensor. With excellent selectivity and stability, these strategies opened up a new avenue for realizing the ultrasensitive detection of PCT and other biomarkers in a real sample analysis. That provided some distinctive angle for extending electrochemical methods to immunoassay.

CRediT authorship contribution statement

Yue Jia: Conceptualization, Data curation, Investigation, Visualization, Writing - original draft. **Lei Yang:** Formal analysis, Methodology. **Jingwei Xue:** Formal analysis, Methodology. **Xiang Ren:** Supervision, Writing - review & editing. **Nuo Zhang:** Supervision, Writing - review & editing. **Dawei Fan:** Supervision, Writing - review & editing. **Qin Wei:** Project administration, Resources. **Hongmin Ma:** Conceptualization, Formal analysis, Methodology, Resources.

Declaration of competing interest

The authors declare that they have no known competing financial interests or personal relationships that could have appeared to influence the work reported in this paper.

Acknowledgments

This study was supported by the National Key Scientifc Instrument and Equipment Development Project of China (No. 21627809), National Natural Science Foundation of China (Nos. 21675063, 21575050, 21777056, 21505051).

Appendix A. Supplementary data

Supplementary data to this article can be found online at https://doi.org/10.1016/j.bios.2019.111676.

References

Bi, S., Yue, S.Z., Zhang, S.S., 2017. Chem. Soc. Rev. 46, 4281–4298.
Bruce, D., Richter, M.M., 2002. Anal. Chem. 74, 1340–1342.
Cabiscol, E., Tamarit, J., Ros, J., 2000. Int. Microbiol. : Off. J. Span. Soc. Microbiol. 3, 3–8.
Chen, Y., Zhao, D.B., Fu, J.J., Gou, X.D., Jiang, D.C., Dong, H., Zhu, J.J., 2019. Anal. Chem. 91, 6829–6835.
Davies, K.J., 1987. J. Biol. Chem. 262, 9895–9901.
Ghrera, A.S., 2019. Anal. Chim. Acta 1056, 26–33.
Grabar, K.C., Brown, K.R., Keating, C.D., Stranick, S.J., Tang, S.L., Natan, M.J., 1997. Anal. Chem. 69, 471–477.
Greenfield, N.J., 2006. Nat. Protoc. 1, 2876–2890.
Guo, X.R., Wu, F.Y., Ni, Y.N., Kokot, S., 2016. Anal. Chim. Acta 942, 112–120.
Jia, Y., Yang, L., Feng, R.Q., Ma, H.M., Fan, D.W., Yan, T., Feng, R., Du, B., Wei, Q., 2019a. ACS Appl. Mater. Interfaces 11, 7157–7163.
Jia, Y., Yang, L., Xue, J., Zhang, N., Fan, D., Ma, H., Ren, X., Hu, L., Wei, Q., 2019b. ACS Sens. 4, 1909–1916.
Klepper, K.B., Nilsen, O., Hansen, P.A., Fjellvag, H., 2011. Dalton Trans. 40, 4636–4646.
Li, H.N., Sun, Y.Y., Elseviers, J., Muyldermans, S., Liu, S.Q., Wan, Y.K., 2014. Analyst 139, 3718–3721.
Li, Y., Huang, C.Z., Li, Y.F., 2019. Anal. Chem. 91, 9308–9314.
Ma, M.N., Zhuo, Y., Yuan, R., Chai, Y.Q., 2015. Anal. Chem. 87, 11389–11397.
Makaraviciute, A., Ramanaviciene, A., 2013. Biosens. Bioelectron. 50, 460–471.
Nhlapo, N.S., Focke, W.W., Vuorinen, E., 2012. Thermochim. Acta 546, 113–119.
Sha, H.F., Zhang, Y., Wang, Y.F., Ke, H., Xiong, X., Jia, N.Q., 2019. Biosens. Bioelectron. 124, 59–65.
Shen, W.J., Zhuo, Y., Chai, Y.Q., Yang, Z.H., Han, J., Yuan, R., 2015. ACS Appl. Mater. Interfaces 7, 4127–4134.
Song, X.Z., Li, X.J., Wei, D., Feng, R., Yan, T., Wang, Y.G., Ren, X., Du, B., Ma, H.M., Wei, Q., 2019. Biosens. Bioelectron. 126, 222–229.
Sun, F., Wang, Z.C., 2019. Mater. Lett. 234, 62–65.
Sun, M.F., Liu, J.L., Chai, Y.Q., Zhang, J., Tang, Y., Yuan, R., 2019. Anal. Chem. 91, 7765–7773.
Wang, C., Zhang, N., Li, Y.Y., Yang, L., Wei, D., Yan, T., Ju, H.X., Du, B., Wei, Q., 2019. Sens. Actuators B Chem. 291, 319–328.
Xie, J., Zheng, Y., Ying, J.Y., 2009. J. Am. Chem. Soc. 131, 888–889.
Yan, M., Ye, J., Zhu, Q., Zhu, L., Huang, J., Yang, X., 2019a. Anal. Chem. 91, 10156–10163.
Yan, Y.C., Li, J., Li, W.H., Wang, Y., Song, W.L., Bi, S., 2018. Nanoscale 10, 22456–22465.
Yan, Y.C., Shi, P.F., Song, W.L., Bi, S., 2019b. Theranostics 9, 4047–4065.
Yang, L., Fan, D.W., Zhang, Y., Ding, C.F., Wu, D., Wei, Q., Ju, H.X., 2019a. Anal. Chem. 91, 7145–7152.
Yang, L., Zhang, B., Fu, L., Fu, K., Zou, G., 2019b. Angew. Chem. Int. Ed. 58, 6901–6905.
Yu, Y.Q., Zhang, H.Y., Chai, Y.Q., Yuan, R., Zhuo, Y., 2016. Biosens. Bioelectron. 85, 8–15.
Zeng, W.J., Liao, N., Lei, Y.M., Zhao, J., Chai, Y.Q., Yuan, R., Zhuo, Y., 2018. Biosens. Bioelectron. 100, 490–496.
Zhang, C., Fan, Y., Zhang, H., Chen, S.H., Yuan, R., 2019a. Anal. Bioanal. Chem. 411, 905–913.
Zhang, X.L., Li, X., Li, X.T., Gao, Y., Feng, F., Yang, G.J., 2019b. Sens. Actuators B Chem. 282, 927–935.
Zhao, M., Chen, A.Y., Huang, D., Chai, Y.Q., Zhuo, Y., Yuan, R., 2017. Anal. Chem. 89, 8335–8342.
Zhou, Y., Chen, S.H., Luo, X.L., Chai, Y.Q., Yuan, R., 2018. Anal. Chem. 90, 10024–10030.